

Metadata Improves Segmentation Through Multitasking Elicitation

Iaroslav Plutenko^{1,2}, Mikhail Papkov³, Kaupo Palo⁴, Leopold Parts^{3,5}, and Dmytro Fishman³

¹ Ukrainian Catholic University, Lviv, Ukraine

² Leibniz Institute of Plant Genetics and Crop Plant Research (IPK), Gatersleben, Germany

³ Institute of Computer Science, University of Tartu, Estonia

⁴ Revvity, Inc., Tallinn, Estonia

⁵ Wellcome Sanger Institute, Hinxton, United Kingdom

plutenko@ipk-gatersleben.de

dmytro.fishman@ut.ee

Abstract. Metainformation is a common companion to biomedical images. However, this potentially powerful additional source of signal from image acquisition has had limited use in deep learning methods, for semantic segmentation in particular. Here, we incorporate metadata by employing a channel modulation mechanism in convolutional networks and study its effect on semantic segmentation tasks. We demonstrate that metadata as additional input to a convolutional network can improve segmentation results while being inexpensive in implementation as a nimble add-on to popular models. We hypothesize that this benefit of metadata can be attributed to facilitating multitask switching. This aspect of metadata-driven systems is explored and discussed in detail.

Keywords: semantic segmentation · metadata · multitasking.

1 Introduction

Semantic segmentation is a technique broadly applied in biomedicine, separating critical regions according to their functional role in the source object, *e.g.*, detecting tumors from CT images [18] or differentiating cell nuclei from the background [2]. When performed by trained human experts, this task is time-consuming and costly [5]. The oldest automated techniques [19,4] in image processing were rule-based routines that separated regions on deterministic criteria. Since then, machine learning methods have taken over the field [8,15]. Most recently, deep learning models eliminated many manual steps in image processing and outperformed previous methods [10], but substantial improvements are still needed for robust systems.

Digital images often come with abundant metainformation reflecting image acquisition device settings, the methodology of sample preparation, or the provenance of the inspected objects. This information alone can say a lot about how images look and their quality, and potentially influence the segmentation

results. For example, different cell lines have distinct appearances under the microscope [2], and knowing which types of cells to look for helps locate them.

Incorporating metadata into computer vision models is straightforward for the classification task. Kawahara *et al.* used a convolutional neural network (CNN) to extract features from skin images and concatenated them with a one-hot encoded metadata vector to analyze lesions [14]. Gessert *et al.* used an additional dense neural network to process age, anatomical site, and sex metadata and fused its features with the CNN [9]. However, mixing non-image data into the fully-convolutional neural network for semantic segmentation is less trivial. De Vries *et al.* introduced Conditional Batch Normalization to integrate additional information into feature maps [7]. This idea was developed into Feature-wise Linear Modulation (FiLM) [21] and Conditioned-U-Net [6]. Later, FiLM was adopted for the biomedical domain [17].

The idea of modulating CNN feature maps closely relates to channel attention, which uses learnable weights to emphasize relevant feature maps. Channel attention is actively employed to improve CNN’s performance [26]. Hu *et al.* introduced a squeeze-and-excitation (SE) block to implement this idea by channel-wise feature recalibration [13]. Lightweight channel modulation blocks were beneficial for CNNs in various tasks [23,3].

This work explores the value of channel attention using SE block for metadata incorporation. We investigate the effects of categorical and continuous metadata on semantic segmentation and show that metadata improves the model’s generalization and overall performance. We conduct experiments on biomedical datasets using metadata such as cell line labels and expected object size. Further, we explore the utility of the metadata to help the model effectively navigate multiple tasks on the same images. The results show a statistically significant advantage of metadata-driven models over metadata-free models. The difference becomes more pronounced when the model is trained on visually similar domains, and the system exhibits its multitasking properties. Overall, our contributions are as follows:

1. We present a novel, simple, lightweight, yet effective metadata-enhanced squeeze-and-excitation block.
2. We empirically show that using metadata improves the performance of the semantic segmentation models.
3. We find that metadata drastically increases the performance for the under-represented task in a multitask setting.

2 Methods

2.1 Metadata incorporation with channel modulation

Squeeze-and-excitation (SE) blocks are a natural place for metadata fusion in a shallow bottleneck for channel recalibration. They consist of two linear layers, with ReLU activation for the first layer and sigmoid activation for the second. Each block’s input is squeezed from feature maps with pooling. The output is multiplied

channel-wise with the same feature maps. We propose two ways of modifying an SE block. First, encoded metainformation can fully replace the squeezed input to the multi-layer perceptron. We call this block metadata-excitation (ME) because we abandon squeezing entirely. Second, we can concatenate metainformation to the squeezed vector allowing the network itself to decide on the importance of each input. We refer to this modification as squeeze-metadata-and-excitation (SME). Here, we test the performance of ME and SME blocks as components of U-Net network architecture against the baseline model with vanilla SE block.

We implement ME and SME blocks as a part of the modified U-Net [22] architecture (Figure 1). The number of inputs depends on the configuration (number of feature maps, metadata elements, and selected type of block). Hidden dimensionality is four times lower than the number of feature maps.

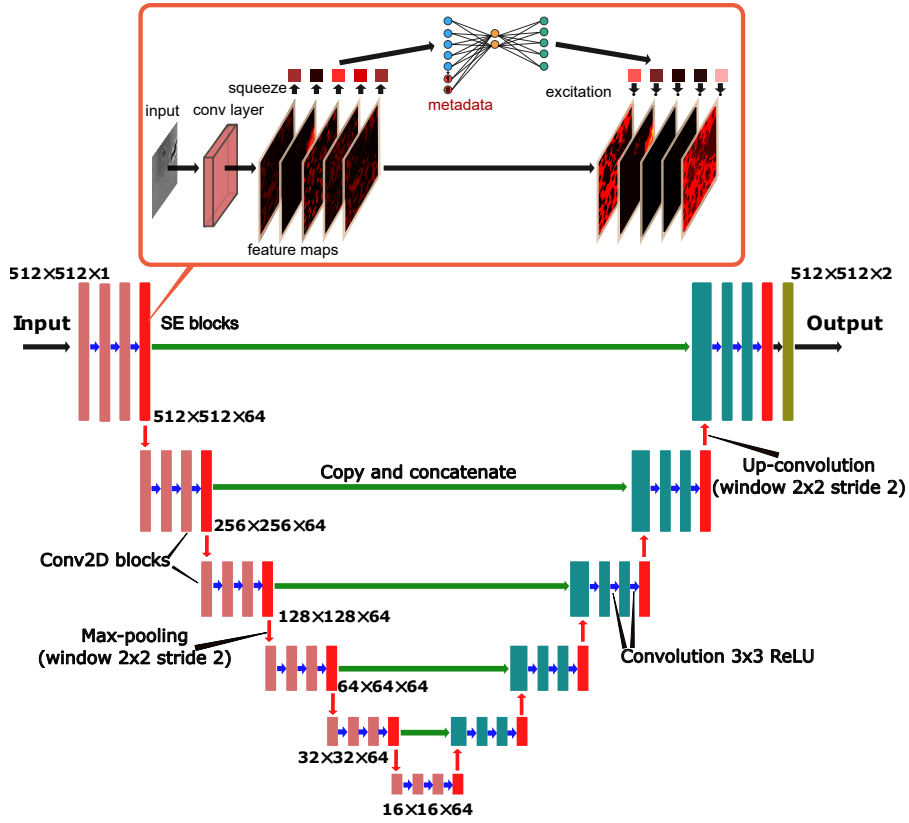


Fig. 1: Integration of metadata into U-Net as an additional block with channel attention functionality that can also receive encoded metadata affecting feature maps intensity. Here the schema for the SME model is shown. For the ME model squeeze part is absent, and the input to the linear layers consists of metadata only (red circles).

2.2 Training

We used Adam optimizer [16] with CyclicLR [24] scheduler changing the learning rate linearly after each batch from 0.0002 to 0.0008 and back in 8 cycles for 100 epochs. We saved the best model by validation error for the downstream analysis. We implemented all the models in PyTorch 1.6 [20] and trained them on NVIDIA Tesla V100 16/32Gb GPUs with cuDNN 7.6.3.

3 Experiments

3.1 Microscopy segmentation across cell lines

To assess the impact of metadata on microscopy image segmentation, we trained our models on the Seven Cell Lines brightfield microscopy dataset [2]. It consists of 3024 samples from seven cell lines in equal proportions: HeLa, MDCK, HepG2, A549, HT1080, MCF7, NIH3T3. Each sample is a single-channel image of size 1080 x 1080 pixels paired with a binary mask of cell nuclei and a metadata vector with a one-hot encoded cell line label (Supplementary Table S1). Part of the models was trained conventionally without access to metadata, and another part had been assisted by metadata labels provided as additional input. Our best models that had access to metadata (SME) had shown an improvement in F_1 score from 0.861 to 0.863 ($p < 0.001$) compared to the baseline model trained without metainformation (Table 1). For comparison, we also used the FiLM model from the `ivadomed` toolbox [11]. It did not outperform the baseline model with an F_1 score of 0.86. Visually the improvements are seen as better overlaps with ground truth masks (Supplementary Figure S1).

	Average	HeLa	MDCK	A549	HT1080	HepG2	MCF7	NIH3T3
baseline stratified	-	<u>0.901</u>	0.830	0.841	0.857	0.806	0.825	<u>0.891</u>
baseline	<u>0.861</u>	<u>0.901</u>	<u>0.865</u>	0.852	<u>0.870</u>	0.806	<u>0.840</u>	<u>0.891</u>
FiLM-dummy [21,6,17]	0.855	0.895	0.858	0.846	0.864	0.802	0.835	0.885
FiLM [21,6,17]	0.860	0.900	<u>0.865</u>	<u>0.853</u>	0.867	0.806	0.839	0.890
ME	<u>0.861</u>	0.900	<u>0.865</u>	0.852	0.869	<u>0.808</u>	0.842	<u>0.891</u>
SME-dummy	0.859	0.899	0.864	0.852	0.867	0.805	0.838	0.889
SME	0.863	0.902	0.869	0.854	0.872	0.809	0.842	0.893

Table 1: Resulting F_1 scores of models trained on the Seven Cell Lines dataset. See Section 2.1 for method description. “baseline stratified” denotes the performance of the models trained on the particular subset of data (cell line), “dummy” denotes metadata vector filled with zeros. The best score is in **bold**, the second best underlined.

3.2 Microscopy segmentation across annotation styles

Microscopists can exhibit different annotation styles when drawing an object boundary as polygon vertices. More points provide more accurate segmentation,

while fewer points save labeling time. From the Seven Cell Lines training dataset we derived a dataset with three nuclei stencil styles using various polygonization degrees of `skimage.measure.approximate_polygon()` [25]. One-third of masks were left unchanged. The second third had a fine approximation to polygons. The remaining part had coarser annotations (Supplementary Figure S2). The test and validation parts had accurate masks and remained consistent with the Seven Cell Lines dataset. Thus, we aimed to obtain fine-grained segmentation results with coarsely annotated parts of the training set.

Here, a metadata label serves as a task identifier, making the model predict masks with shape and confidence specific to the annotation style. The coarse style lowers the prediction confidence, affecting the area of the binarized mask. Switching the model to the mode with accurate masks during the evaluation boosts confidence and helps increase accuracy on the test set (Supplementary Figure S3). All models with metadata had higher F_1 scores, with improvements from 0.846 to 0.854 with our best SME model compared to the baseline model trained on all three parts of the dataset without metadata ($p < 0.001$, Table 2).

	F_1 score
baseline 1/3 data	0.837
baseline	0.846
ME	<u>0.850</u>
SME	0.854
FiLM	0.849
SME dummy	0.848

Table 2: Results of the experiment with the dataset with different annotation styles. Row “baseline 1/3” denotes results from the SE model trained on one-third of data with accurate masks. The main baseline model was trained on the full dataset without metadata. ME, SME, and FiLM models use metadata with different implementations. SME dummy - SME model with meaningless metadata (zeros in the input vector). The best score is in **bold**, the second best underlined.

3.3 Microscopy multilabel segmentation: cells and anomalies

Researchers prefer a clean dataset, as visual artifacts hinder downstream analysis [1]. However, anomaly segmentation for microscopy remains a challenging task because of the lack of annotations and their diverse shapes and sizes. We propose to take advantage of nuclei mask abundance and use metadata as a switch for multitask learning. Thus, we train the network to produce nuclei and anomaly segmentation from a single head, depending on the metadata input. To assess this approach and compare it with a conventional parallel multi-headed prediction, we expand the Seven Cell Lines dataset with multilabel targets. For 365 images out of 3024, we additionally present anomaly segmentation masks,

highlighting debris and optical defects. For these images, metadata encodes the mask type: nuclei or anomaly. Since anomaly annotations are absent for the rest of the dataset, we are able to train parallel multi-headed networks only on this subset with two segmentation masks. On the contrary, we can train on the whole dataset when using metadata as a task switch.

A metadata-driven model achieved an F_1 score of 0.836 and 0.85 for nuclei and anomalies, respectively (Table 3). It notably outperformed the baseline model trained to segment only anomalies that had F_1 score of 0.736 on the anomaly subset. At the same time, the performance for nuclei segmentation slightly dropped from the baseline F_1 score of 0.854 on the nuclei subset. Expectedly, swapping metadata labels resulted in segmentation failure, approaching zero F_1 score. The model with dummy metadata input also struggled with anomaly segmentation due to the dominance of nuclei masks, predicting only nuclei.

Additionally, we utilized a limited version of the large dataset containing nuclei and anomalies on the same images. Training a multi-headed model parallelly on this reduced dataset, with each head’s output corresponding to a different mask, yielded a higher F_1 score of 0.835 on the anomaly subset than the baseline model with F_1 score of 0.736 training exclusively on that subset. The performance on the nuclei mask subset was lower due to the limited training size (the stratified baseline model trained on a limited subset of nuclei was not introduced in this experiment due to the focus on anomaly segmentation).

Surprisingly, when our initial metadata-driven model with a single output was retrained on the reduced dataset in the usual sequential mode using metadata to switch segmentation task, the anomaly subset showed the highest boost in F_1 score among all experiments: 0.854 compared to the individual model with F_1 score of 0.736. Detailed results are summarized in Table 3.

		Average Anomalies Seven Cell Lines		
Full dataset	baseline stratified	-	0.736	0.854
	ME	0.835	0.824	0.845
	SME-dummy	0.470	0.104	0.835
	SME	0.843	<u>0.836</u>	0.850
Multilabel subset	Two heads	0.812	0.835	0.789
	SME	0.823	0.854	0.792

Table 3: F_1 scores for multitask models from experiments on dataset with anomalies (full and multilabel subset). See Section 2.1 for method description. “baseline stratified” denotes the performance of the SE models trained on the particular subset of data (anomaly/nuclei masks), “dummy” denotes the model with metadata vector filled with zeros. The best score is in **bold**, the second best underlined.

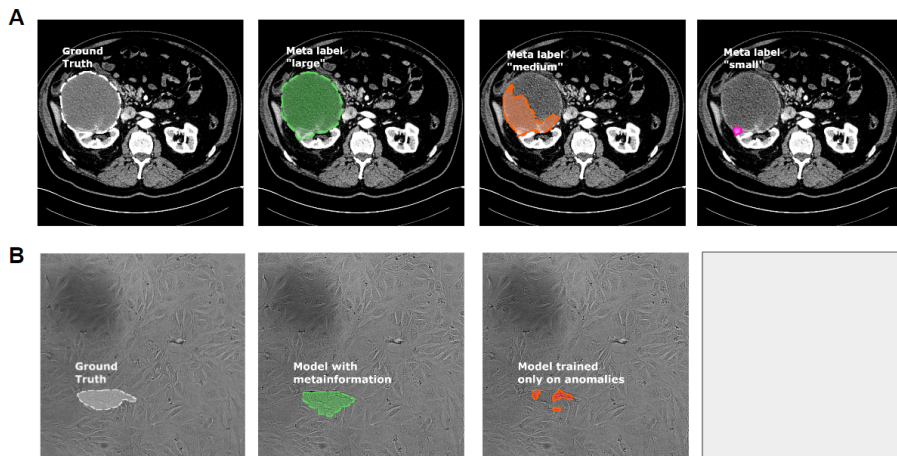


Fig. 2: (A) Manifestation of multitask properties in metadata-driven models with continuous metadata correlated with the tumor size on KiTS21 dataset. In this experiment, the baseline model had on the test F_1 score of 0.734, and metadata-driven models (SME and ME) had an average F_1 score of 0.804 for two models. (B) Example of positive transfer for the anomaly segmentation task with the metadata-driven model — the baseline model (trained only on the anomaly subset) had F_1 score of 0.736 on this subset, metadata-driven models (SME) had F_1 score of 0.854 on anomaly subset.

3.4 Kidney tumor segmentation with continuous metadata

To test our method’s applicability for continuous metadata, we used KiTS21 [12] 3D dataset of 200 images accompanied with the tumor size information. We derived a 2D dataset from it with 10346 images selecting axial slices containing kidneys. Segmentation targets contain three classes: kidney tissue, tumor, and cyst (cyst and tumors were exclusive classes — cases with tumors did not have cysts and vice versa). In this experiment, the baseline model had a F_1 score of 0.734 on the test, metadata-driven model ME achieved a F_1 score of 0.807, and another metadata-driven SME model achieved a F_1 score of 0.801. In Figure 2A, we illustrate how the target mask changes in response to different size-correlated metadata applied to the same image.

4 Discussion

Metadata is a widely available and potentially valuable source of additional information for deep learning systems. We used a channel modulation mechanism to inject it into the image-processing workflow, a lightweight and low-intrusive approach for adapting existing CNNs. Despite small dimensionality compared to the main input, metadata can drastically change the course of learning and inference by indicating the presence of a specific task. Our experiments show

how this change is especially obvious when no other visual clues are present in the image. The results demonstrate that the CNN models endowed with metadata awareness respond strongly to the metadata input, adjusting their output according to the respective task indicator. While the correct metadata labels improve the segmentation performance, providing incorrect labels significantly hinders the model’s functionality. The metadata-driven system inherently has a multitasking nature that allows exploiting the benefits of combining several tasks. Our results for segmenting anomalies and nuclei from microscopy images confirm these assumptions.

We have proposed a method of incorporating metadata from a variety of sources into an image segmentation pipeline and demonstrated its effectiveness. We showed that metadata can act as a guiding label (in both discrete and continuous form) or even as a task switch. We believe that principles of multi-task learning, some of which we have uncovered here, will remain universal for metadata-driven segmentation systems and persist regardless of chosen implementation and architecture. Ultimately, metadata could be the unifying modality that allows training truly cross-domain models.

Acknowledgements This work was funded by Revvity, Inc. (previously known as PerkinElmer Inc., VLTAT19682), and Wellcome Trust (206194). We thank High Performance Computing Center of the Institute of Computer Science at the University of Tartu for the provided computing power.

References

1. Ali, M.A.S., Hollo, K., Laasfeld, T., Torp, J., Tahk, M.J., Rinken, A., Palo, K., Parts, L., Fishman, D.: ArtSeg: Rapid artifact segmentation and removal in brightfield cell microscopy images (Jan 2022)
2. Ali, M.A.S., Misko, O., Salumaa, S.O., Papkov, M., Palo, K., Fishman, D., Parts, L.: Evaluating very deep convolutional neural networks for nucleus segmentation from brightfield cell microscopy images. *SLAS Discov* **26**(9), 1125–1137 (Oct 2021)
3. Amer, A., Ye, X., Zolgharni, M., Janan, F.: ResDUnet: Residual dilated UNet for left ventricle segmentation from echocardiographic images. *Conf. Proc. IEEE Eng. Med. Biol. Soc.* **2020**, 2019–2022 (Jul 2020)
4. Beucher, S.: Use of watersheds in contour detection. *Proc. Int. Workshop on Image Processing*, Sept. 1979 pp. 17–21 (1979)
5. Bhalgat, Y., Shah, M., Awate, S.: Annotation-cost minimization for medical image segmentation using suggestive mixed supervision fully convolutional networks (Dec 2018)
6. Brocal, G.M., Peeters, G.: Conditioned-U-Net: Introducing a control mechanism in the U-Net for multiple source separations. In: *Proceedings of the 20th International Society for Music Information Retrieval Conference*. Zenodo (2019)
7. De Vries, H., Strub, F., Mary, J., Larochelle, H., Pietquin, O., Courville, A.C.: Modulating early visual processing by language. *Adv. Neural Inf. Process. Syst.* **30** (2017)

8. Georgiou, T., Liu, Y., Chen, W., Lew, M.: A survey of traditional and deep learning-based feature descriptors for high dimensional data in computer vision. *International Journal of Multimedia Information Retrieval* **9**(3), 135–170 (Sep 2020)
9. Gessert, N., Nielsen, M., Shaikh, M., Werner, R., Schlaefler, A.: Skin lesion classification using ensembles of multi-resolution EfficientNets with meta data. *MethodsX* **7**, 100864 (Mar 2020)
10. Greenspan, H., van Ginneken, B., Summers, R.M.: Guest editorial deep learning in medical imaging: Overview and future promise of an exciting new technique. *IEEE Trans. Med. Imaging* **35**(5), 1153–1159 (May 2016)
11. Gros, C., Lemay, A., Vincent, O., Rouhier, L., Bourget, M.H., Bucquet, A., Cohen, J., Cohen-Adad, J.: Ivadomed: A medical imaging deep learning toolbox. *J. Open Source Softw.* **6**(58), 2868 (Feb 2021)
12. Heller, N., Isensee, F., Maier-Hein, K.H., Hou, X., Xie, C., Li, F., Nan, Y., Mu, G., Lin, Z., Han, M., Yao, G., Gao, Y., Zhang, Y., Wang, Y., Hou, F., Yang, J., Xiong, G., Tian, J., Zhong, C., Ma, J., Rickman, J., Dean, J., Stai, B., Tejpaul, R., Oestreich, M., Blake, P., Kaluzniak, H., Raza, S., Rosenberg, J., Moore, K., Walczak, E., Rengel, Z., Edgerton, Z., Vasdev, R., Peterson, M., McSweeney, S., Peterson, S., Kalapara, A., Sathianathen, N., Papanikolopoulos, N., Weight, C.: The state of the art in kidney and kidney tumor segmentation in contrast-enhanced CT imaging: Results of the KiTS19 challenge. *Med. Image Anal.* **67**, 101821 (Jan 2021)
13. Hu, J., Shen, L., Albanie, S., Sun, G., Wu, E.: Squeeze-and-Excitation networks. *IEEE Trans. Pattern Anal. Mach. Intell.* **42**(8), 2011–2023 (Aug 2020)
14. Kawahara, J., Daneshvar, S., Argenziano, G., Hamarneh, G.: 7-point checklist and skin lesion classification using Multi-Task Multi-Modal neural nets. *IEEE J Biomed Health Inform* (Apr 2018)
15. Khan, S., Sajjad, M., Hussain, T., Ullah, A., Imran, A.S.: A review on traditional machine learning and deep learning models for WBCs classification in blood smear images. *IEEE Access* **9**, 10657–10673 (2021)
16. Kingma, D.P., Ba, J.: Adam: A method for stochastic optimization (Dec 2014)
17. Lemay, A., Gros, C., Vincent, O., Liu, Y., Cohen, J.P., Cohen-Adad, J.: Benefits of linear conditioning for segmentation using metadata. In: Heinrich, M., Dou, Q., de Bruijne, M., Lellmann, J., Schläfer, A., Ernst, F. (eds.) *Proceedings of the Fourth Conference on Medical Imaging with Deep Learning. Proceedings of Machine Learning Research*, vol. 143, pp. 416–430. PMLR (2021)
18. Litjens, G., Kooi, T., Bejnordi, B.E., Setio, A.A.A., Ciampi, F., Ghafoorian, M., van der Laak, J.A.W.M., van Ginneken, B., Sánchez, C.I.: A survey on deep learning in medical image analysis. *Med. Image Anal.* **42**, 60–88 (Dec 2017)
19. Otsu, N.: A threshold selection method from gray-level histograms. *IEEE Trans. Syst. Man Cybern.* **9**(1), 62–66 (Jan 1979)
20. Paszke, A., Gross, S., Massa, F., Lerer, A., Bradbury, J., Chanan, G., Killeen, T., Lin, Z., Gimelshein, N., Antiga, L., et al.: Pytorch: An imperative style, high-performance deep learning library. In: *Advances in neural information processing systems*. pp. 8026–8037 (2019)
21. Perez, E., Strub, F., de Vries, H., Dumoulin, V., Courville, A.: FiLM: Visual reasoning with a general conditioning layer. *AAAI* **32**(1) (Apr 2018)
22. Ronneberger, O., Fischer, P., Brox, T.: U-Net: Convolutional networks for biomedical image segmentation. In: *Medical Image Computing and Computer-Assisted Intervention – MICCAI 2015*. pp. 234–241. Springer International Publishing (2015)
23. Roy, S.K., Dubey, S.R., Chatterjee, S., Chaudhuri, B.B.: FuSENet: fused squeeze-and-excitation network for spectral-spatial hyperspectral image classification (2020)

24. Smith, L.N.: Cyclical learning rates for training neural networks. In: 2017 IEEE Winter Conference on Applications of Computer Vision (WACV). pp. 464–472 (Mar 2017)
25. Van der Walt, S., Schönberger, J.L., Nunez-Iglesias, J., Boulogne, F., Warner, J.D., Yager, N., Gouillart, E., Yu, T.: scikit-image: image processing in python. *PeerJ* **2**, e453 (2014)
26. Woo, S., Park, J., Lee, J.Y., Kweon, I.S.: CBAM: Convolutional block attention module. In: *Computer Vision – ECCV 2018*, pp. 3–19. *Lecture notes in computer science*, Springer International Publishing, Cham (2018)

Supplementary materials

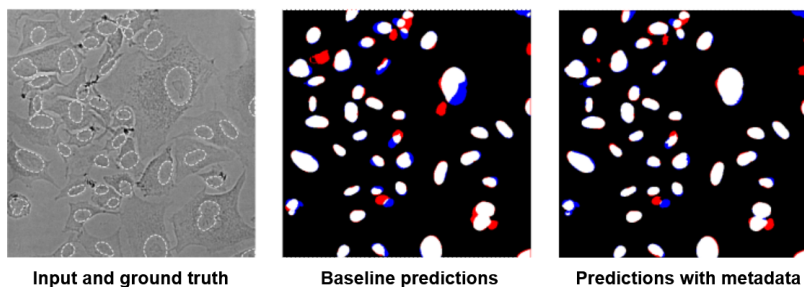


Fig. S1: Models with metadata perform better. An example of a prediction of the A549 sample from the original Seven Cell Lines dataset mapped to the ground truth mask, where pixel color represents **false positive**, **false negative**, and white denotes the correct match with ground truth. The baseline model has an average F_1 score of 0.861, metadata-driven SME model has an average F_1 score of 0.863

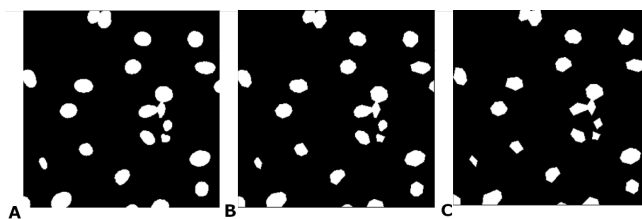


Fig. S2: Simplified polygonized masks from cell lines dataset to imitate annotation style. Original masks (A) were polygonized with high approximation using the `tolerance=2` in `skimage.measure.approximate_polygon()` (B) and lower approximation with the `tolerance=3.5`(C).

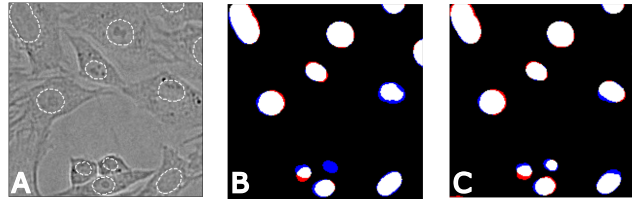


Fig. S3: Prediction with metadata corresponding to accurate masks improves segmentation with more accurate stencils shape and confidence. Example of performance on a sample patch from the test data. Source image with ground truth contours (A), masks from baseline model (B), which has a test set F_1 score of 0.846, and masks from the SME model in the inference mode with metadata corresponding to accurate masks (C), having a test set F_1 score of 0.854. The color represents false positive and false negative pixels and the white color denotes the correct match with ground truth.

	A549	HT1080	HeLa	HepG2	MCF7	MDCK	NIH3T3	Polygons	Anomalies
Train	286	284	293	283	290	292	288	672/672/672	194
Val	66	78	58	82	70	79	71	504	70
Test	80	70	81	67	72	61	73	504	101

Table S1: Datasets distribution. For the dataset with polygonized masks the distribution between accurate masks, fine and coarse polygons in the train set are shown, while the validation and test sets contain accurate masks